RSC Advances

PAPER

View Article Online
View Journal | View Issue

Open Access Article. Published on 11 July 2017. Downloaded on 1/9/2026 1:23:19 AM.
This article is licensed under a Creative Commons Attribution-NonCommercial 3.0 Unported Licence.

Check for updates

Cite this: *RSC Adv.*, 2017, **7**, 34530

Methane combustion over $Pd/CoAl_2O_4/Al_2O_3$ catalysts prepared by galvanic deposition†

Yuji Mahara,[a] Takumi Tojo,[a] Kazumasa Murata,[a] Junya Ohyama[ab] and Atsushi Satsuma*[ab]

Received 2nd June 2017
Accepted 3rd July 2017

DOI: 10.1039/c7ra06150a

rsc.li/rsc-advances

$Pd/CoAl_2O_4/Al_2O_3$ methane combustion catalysts were synthesized using a galvanic deposition (GD) method (PdCoAl-GD). This PdCoAl-GD catalyst showed higher activities and turnover frequencies (TOFs) than conventional Pd/Al_2O_3. According to X-ray diffraction (XRD), X-ray absorption fine structure (XAFS) and scanning transmission electron microscopy (STEM) measurements, PdCoAl-GD was composed of a $CoAl_2O_4$ phase supported on γ-Al_2O_3 and dispersed Pd nanoparticles of 2–7 nm in size on $CoAl_2O_4$. Operando Pd K-edge XAFS measurements indicated that the Pd in PdCoAl-GD was oxidized to highly active methane combustion PdO species at low temperatures. PdCoAl-GD also showed high activity (light-off tests) when PdO was initially present on the catalysts. Methane temperature-programmed reaction (CH_4-TPR) measurements on PdCoAl-GD revealed that PdO was reduced by CH_4 at low temperatures. The GD method used herein achieved PdO species that were effective for C–H activation.

Introduction

Natural gas vehicles are becoming widely used because of their cleaner exhaust gas characteristics compared to conventional fossil fuel-based automobiles. However, unburned methane emissions are hazardous and have a high greenhouse effect coefficient that is 21 times higher than carbon dioxide. Complete oxidation of methane using supported heterogeneous catalysts has become increasingly important for emission reduction of unburned methane.[1–3] Supported Pd catalysts have been used because of their high activity in methane combustion,[4–37] and alumina-supported Pd catalysts (Pd/Al_2O_3) are used, especially, due to their high activity and thermal stability. However, methane combustion activity at low temperatures is still insufficient and the development of a highly active catalyst at low temperatures is strongly desired.

For the aim of designing catalysts with higher activity, it is important to control the Pd–metal oxide interaction. Cargnello *et al.* synthesized $Pd@CeO_2$ catalysts that have attracted attention because of their exceptional methane combustion activities,[36] and the influence of the Pd–CeO_2 interfaces on high methane combustion activity has been experimentally and theoretically studied.[7,38,39] Zou *et al.* prepared alumina-supported core–shell NiO@PdO catalysts with higher Pd utilization efficiencies than Pd/CeO_2. However, these catalysts were prepared by a complex method (*i.e.*, multi-step reactions and protecting agents); thus, a simpler preparation method is desired. The addition of transition metal (*e.g.*, Ni or Co) oxides to Pd/Al_2O_3 catalysts has been reported to improve their methane combustion activity.[4,6,13,23,25,30,32] However, to improve the activity, Pd is required to be in good contact with the additional element species. In this sense, we used a galvanic deposition (GD) method to enhance the interaction between Pd and CoO_x species.[21] The GD method allowed the support of a metal over a second metal with a higher ionization tendency. Thus, different metals were deposited upon contact between the two metals, thereby enhancing their interfacial interaction. Pd–Co/Al_2O_3 catalysts prepared by a GD method showed significantly higher methane combustion activities compared to Pd/Al_2O_3 and Pd–Co/Al_2O_3 prepared by a conventional impregnation method. However, this improvement in activity was insufficient because of the poor contact between Pd and the relatively large Co particles. The interfacial contact between Pd and Co is expected to improve by precipitating Pd with a GD method after dispersion of Co in a solid solution in Al_2O_3.

In this study, we synthesized highly active $Pd/CoAl_2O_4/Al_2O_3$ methane combustion catalysts with enhanced interfacial contact between Pd and $CoAl_2O_4$ using a GD method. The oxidation state of Pd during the reaction was observed *in situ* by operando X-ray absorption fine structure (XAFS) spectroscopy.

Experimental section

Catalyst preparation

$Co(NO_3)_2 \cdot 6H_2O$ (98%) was purchased from Kishida Chemical. A 4.5 wt% $Pd(NO_3)_2$ aqueous solution and high purity Al_2O_3 (99%) were supplied from Cataler Corporation and SASOL, respectively.

[a]*Graduate School of Engineering, Nagoya University, Nagoya 464-8603, Japan. E-mail: satsuma@chembio.nagoya-u.ac.jp*

[b]*Unit of Elements Strategy Initiative for Catalysts & Batteries, Kyoto University, Kyoto 615-8530, Japan*

† Electronic supplementary information (ESI) available. See DOI: 10.1039/c7ra06150a

This journal is © The Royal Society of Chemistry 2017

Open Access Article. Published on 11 July 2017. Downloaded on 1/9/2026 1:23:19 AM.
This article is licensed under a Creative Commons Attribution-NonCommercial 3.0 Unported Licence.

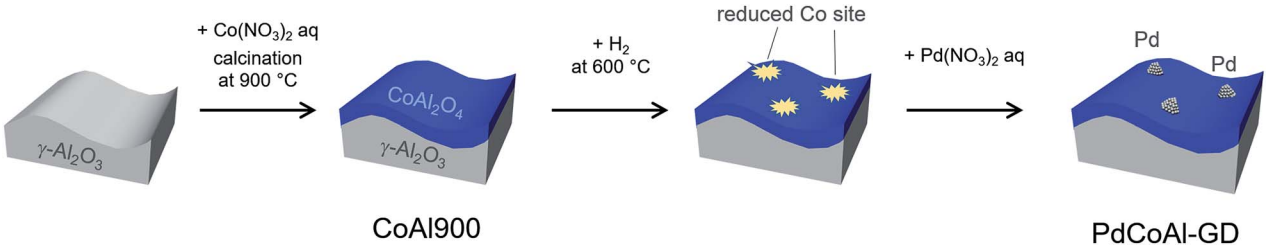

Scheme 1 Synthetic procedure for $Pd/CoAl_2O_4/Al_2O_3$ using galvanic deposition method.

$CoAl_2O_4/Al_2O_3$ (5 wt% Co loading) was prepared by an impregnation method. An aqueous suspension containing boehmite and $Co(NO_3)_2 \cdot 2H_2O$ was stirred for 1 h. After evaporation and overnight drying at 80 °C, the resulting solid was calcined at 900 °C for 3 h. The solid was denoted as CoAl900.

$Pd/CoAl_2O_4/Al_2O_3$ was prepared with CoAl900 and $Pd(NO_3)_2$ by a GD method as described in previous reports (Scheme 1).[21,40–42] 2.5 g of CoAl900 was added to a two-neck round-bottom flask that was capped with a septum. CoAl900 was reduced under flowing H_2 at 600 °C for 30 min. After switching to N_2, the two-neck round-bottom flask containing CoAl900 was kept at 60 °C. 40 mL of degassed H_2O was added to a two-neck round-bottom flask under stirring and 0.478 mmol of aqueous $Pd(NO_3)_2$ was subsequently injected. The slurry was stirred for 1 h, centrifuged, and dried overnight. The resulting material was denoted as PdCoAl-GD. Inductively coupled plasma analysis revealed a Pd loading of 1.9 wt% on PdCoAl-GD, which was equal to the nominal loading. The Co loading was lower than that of CoAl900 (4.7 *vs.* 5.0 wt%), thereby revealing that a fraction of Co was dissolved into water during deposition of Pd.

As a reference catalyst, Pd/Al_2O_3 was prepared by a conventional impregnation method using a $Pd(NO_3)_2$ solution and Al_2O_3. The mixture was dried and calcined in air at 500 °C for 3 h (denoted as PdAl-I). A $Pd/CoAl_2O_4/Al_2O_3$ catalyst was also prepared by a sequential impregnation method using a $Pd(NO_3)_2$ solution and CoAl900. The mixture was dried and calcined in air at 500 °C for 3 h (denoted as PdCoAl-SI). The Pd and Co loadings of the catalysts were adjusted to 2 and 4.9 wt%, respectively.

Catalytic tests

Light-off methane combustion tests were conducted using a conventional fixed-bed flow reactor at atmospheric pressure with 20 mg of catalyst loaded in a Pyrex glass tube with an internal diameter of 4 mm. In this study, we performed catalytic tests under two pretreatment conditions: (i) O_2 at 500 °C for 10 min, followed by a H_2 treatment at 500 °C for 10 min (initial state of Pd : Pd^0); and (ii) O_2 treatment at 500 °C for 10 min (initial state of Pd : PdO). The catalytic tests were performed under flowing (100 mL min^{-1}) 0.4% CH_4/10% O_2/He balance. The reaction temperature ranged from 200 to 600 °C, and the heating rate was 5 °C min^{-1}. The gas hourly space velocity was 300 000 mL (h $g_{cat})^{-1}$. The effluent gas was analyzed by a nondispersive infrared (NDIR) CO/CO_2 analyzer (Horiba VIA510) while stepwise increasing the reaction temperature.

Catalyst characterization

The prepared catalysts were characterized by X-ray diffraction (XRD), XAFS, high-angle annular dark-field scanning transmission electron microscopy (HAADF-STEM), X-ray photoelectron spectroscopy (XPS), CO adsorption, as well as methane temperature-programmed reductions (CH_4-TPR).

The XRD patterns of the catalysts were recorded on a Rigaku MiniFlex II/AP diffractometer with a Cu Kα radiation. All samples were measured after preparation without performing any pretreatment.

The Co K-edge XAFS spectra were obtained on the BL01B1 beamline at the SPring-8 synchrotron radiation facility (8 GeV, 100 mA) of the Japan Synchrotron Radiation Research Institute (JASRI) in Hyogo, Japan. The XAFS measurements (transmission mode) were performed ex situ. The samples were pelletized (7 mm in diameter). PdCoAl-GD and PdCoAl-SI were ex situ measured after methane combustion tests at 600 °C, while CoAl900 was measured after no pretreatment. The data analysis was performed using the Athena and Artemis softwares including in the Demeter package. The curve-fitting analysis of the EXAFS spectra was performed for the inverse Fourier transforms assuming single scattering using the theoretical parameters calculated by FEFF6. The Co K-edge EXAFS data were fitted between 3–12 Å in *k* space and 1–3 Å in *R* space.

HAADF-STEM and energy dispersive X-ray (EDX) images were collected using a JEOL JEM-2100F microscope operating at 200 kV. For TEM analysis, the spent catalysts were dispersed in methanol and dropped onto a Cu mesh provided with a carbon microgrid.

XPS measurements were performed on a JPS-9000MC system (JEOL Ltd.) with Mg Kα radiation to understand the electronic properties of the Pd surface after methane combustion. Because the peak position of the Pd^{2+} $3d_{5/2}$ derived from PdO bulk was 337.3 eV, this value was fit to Pd^{n+} without constraint conditions. The Pd^{2+} $3d_{3/2}$ and Pd^{n+} $3d_{3/2}$ peaks were analyzed considering that the area of this peak was two-thirds of that of $3d_{5/2}$ and four analysis peaks were obtained.

CO chemisorption was carried out on a BELCAT (Bel Japan Inc.) apparatus, while CH_4-TPR was carried out using a NDIR CO/CO_2 analyzer (Horiba VIA510). CO chemisorption was performed after oxidation (O_2 at 500 °C) and reduction (H_2 at 50 °C) pretreatments. For the CH_4-TPR measurements, 50 mg of the sample were heated from 200 to 600 °C at a rate of 5 °C min^{-1} under flowing 0.4% CH_4 in N_2 (50 mL min^{-1}) after a pretreatment with flowing O_2 at 500 °C.

Open Access Article. Published on 11 July 2017. Downloaded on 1/9/2026 1:23:19 AM.
This article is licensed under a Creative Commons Attribution-NonCommercial 3.0 Unported Licence.

Operando Pd K-edge XAFS spectroscopy

Operando Pd K-edge XAFS measurements were performed at BL01B1, SPring-8, Japan. The samples were pelletized (7 mm in diameter) and set in a quartz glass XAFS cell. The measurement sequence was carried out at the same conditions employed for the methane combustion catalytic tests. Thus, after a pretreatment with flowing O_2 (500 °C) and H_2 (500 °C), the catalyst was contacted with flowing 0.4% CH_4/10% O_2/He (reaction mixture) and heated at a rate of 5 °C min^{-1} from 200 to 500 °C. During this heating, quick Pd K-edge XAFS spectra were obtained in a transmission mode. In addition, the composition (*i.e.*, CH_4, CO, CO_2, H_2O, O_2, *etc.*) of the outlet gas was analyzed by mass spectrometry (MS).

Results and discussion

Catalytic activity

We performed methane combustion tests on the prepared catalysts. The catalysts were H_2 pretreated at 500 °C to reduce the Pd species to a metallic phase. Fig. 1(a) shows the light-off methane combustion curves for PdCoAl-GD, PdCoAl-SI, PdAl-I, and CoAl900. T_{10} was defined as the temperature at which methane conversion reached 10%. As shown in Table 1, PdCoAl-GD showed the best low-temperature combustion activity because its T_{10} (266 °C) was *ca.* 20 °C lower than those of PdAl-I and PdCoAl-SI. T_{10} of PdCoAl-SI was slightly lower than that of PdAl-I. Compared with the catalysts previously reported, PdCoAl-GD showed comparable high activity (Table 2 and Fig. S1†).[4,5,7,11,22,24,33,36,43] The apparent activity followed a different trend PdAl-I > PdCoAl-SI at high temperatures. CoAl900 showed no catalytic activity below 400 °C, thereby suggesting that Pd species were the active sites in this reaction.

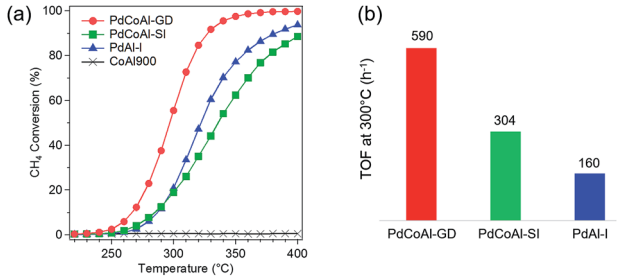

Fig. 1 (a) Methane combustion light-off curves of PdCoAl-GD, PdCoAl-SI, PdAl-I and CoAl900. Pretreatment: flowing O_2 at 500 °C followed by flowing H_2 at 500 °C. (b) Methane combustion TOF at 300 °C over PdCoAl-GD, PdCoAl-SI and PdAl-I.

Table 2 Methane combustion activities for representative catalysts

Catalysts	Reaction rate[a] (μmol_{CH_4} g_{cat}^{-1} s^{-1})	Pd mass activity[a] ($10 \times \mu mol_{CH_4}$ g_{Pd}^{-1} s^{-1})	Ref.
PdCoAl-GD (this work)	8.3	42	—
3% Pd/CeO_2-os	7.4	25	24
Pd@CeO_2/H–Al_2O_3	5.1	51	36
Co@C	1.8	—	43
1.09 wt% Pd/CeO_2	1.5	14	7
Pd/H-ZMS-5(8.0)	1.5	24	5
Pd/Ni–Al_2O_3-GD	1.3	2.6	33
Pd/Co_3O_4–P	1.3	12	11
Pd/Co_3O_4–F	1.2	11	11
1.93$AuPd_{1.95}$/3DOM $CoCr_2O_4$	0.6	—	22
NiO@PdO/Al_2O_3(2 : 1)	0.3	14	4

[a] All value is estimated from the results of methane combustion at 300 °C.

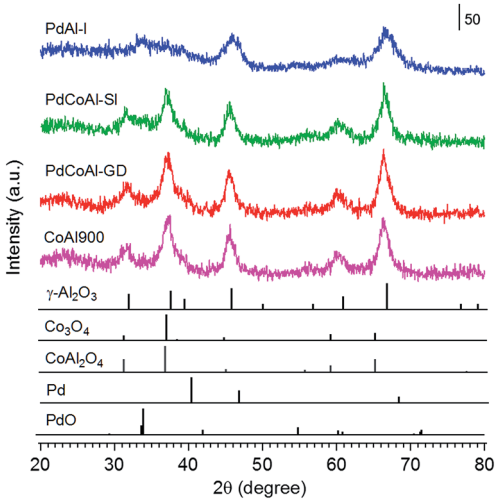

Fig. 2 X-ray diffraction patterns of: PdCoAl-GD, PdCoAl-SI, PdAl-I and CoAl900. The bottom peaks indicate the position of the reference materials.

The turnover frequencies (TOFs) for the prepared catalysts were estimated by the following equation:

$$\mathrm{TOF} = \frac{\text{reaction rate at 300 °C [mol h}^{-1}]}{\text{number of surface Pd [mol]}}$$

Table 1 Catalytic test, CO uptake, Pd particle size, and TOF results

Catalysts	T_{10} (°C)	CO uptake[a] (10^{-6} mol g^{-1})	d_{Pd-CO}[b] (nm)	d_{Pd-TEM} (nm)	TOF at 300 °C (h^{-1})
PdCoAl-GD	266	48.5	4.3	4.2	590
PdCoAl-SI	285	33.5	6.3	6.2	304
PdAl-I	288	57.6	3.8	4.2	160

[a] CO uptake was measured by CO chemisorption after an oxidation pretreatment with O_2 at 500 °C and reduction with H_2 at 50 °C. [b] The Pd particle size was estimated by assuming a CO to surface metal atom ratio of 1 : 1.

 This journal is © The Royal Society of Chemistry 2017

Open Access Article. Published on 11 July 2017. Downloaded on 1/9/2026 1:23:19 AM.
This article is licensed under a Creative Commons Attribution-NonCommercial 3.0 Unported Licence.

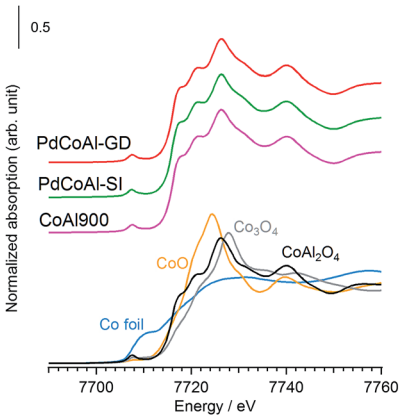

Fig. 3 Normalized absorption spectra at the Co K-edge for PdCoAl-GD (red), PdCoAl-SI (green), CoAl900 (pink) and references (Co foil: royal blue, CoO: orange, Co_3O_4: gray and $CoAl_2O_4$: black).

The number of surface Pd atoms was estimated from the CO chemisorption data. The diameter of the Pd particles obtained by CO chemisorption was also confirmed by the particle size distribution obtained from the HAADF-STEM images. The CO uptake, Pd particle size and TOF values at 300 °C for the catalysts are summarized in Fig. 1(b) and Table 1. The TOF at 300 °C for methane combustion followed the trend PdCoAl-GD > PdCoAl-SI > PdAl-I. The TOF of PdCoAl-GD (590 h^{-1}) was twice that of PdCoAl-SI (304 h^{-1}), and four times higher than that of PdAl-I (160 h^{-1}). PdCoAl-GD, PdCoAl-SI and PdAl-I were estimated to have average Pd particle sizes of 4.3, 6.3 and 3.8 nm, respectively. According to a previous work, catalysts having large sized Pd particles exhibited higher TOFs for methane combustion.[37] Therefore, we prepared several Pd/Al_2O_3 and $Pd/Co/Al_2O_3$ catalysts with varying Pd particle sizes, and we measured the TOF values of these catalysts (Table S1†). PdCoAl-GD showed a noticeably high TOF even considering the Pd size effects (Fig. S2†). Considering the above data, PdCoAl-GD was particularly active toward the methane combustion reaction in the low-temperature range.

Catalyst structure

The catalyst structure was characterized by XRD, XAFS spectroscopy and HAADF-STEM observations.

Fig. 2 shows the XRD patterns of the prepared catalysts. The diffraction patterns confirmed the presence of a γ-Al_2O_3 phase in all cases. Since the diffraction lines originated from Pd were hardly observed, we assumed that Pd was in the form of highly dispersed nanoparticles. The samples containing Co showed XRD patterns characteristics of Co_3O_4 or $CoAl_2O_4$ phases, although we could not discriminate between these structures. Therefore, to investigate the surrounding structure of Co in more detail, XAFS measurements were carried out. Fig. 3 shows the normalized Co K-edge X-ray absorption near-edge spectroscopy (XANES) spectra for PdCoAl-GD, PdCoAl-SI, CoAl900, and reference materials. All the prepared catalysts showed XANES spectra similar to that of $CoAl_2O_4$. Fig. 4 shows the k^3-weighted Co K-edge EXAFS spectra of CoAl900, PdCoAl-GD, PdCoAl-SI, and reference materials. CoAl900, PdCoAl-GD and PdCoAl-SI showed EXAFS spectra similar to that of $CoAl_2O_4$ (and not Co_3O_4). The curve-fitting results of PdCoAl-GD are shown in Table 3. The spectra of PdCoAl-GD showed a first peak at 1.6 Å originated by the Co–O shell and a second peak at 3.0 Å ascribed to the Co–Al, Co–O and Co–Co shells of $CoAl_2O_4$ (Table 3). CoAl900 and PdCoAl-SI also showed spectra similar to that of $CoAl_2O_4$. These results indicated that Co in CoAl900 was almost completely dissolved into the γ-Al_2O_3 phase upon calcination at 900 °C forming a $CoAl_2O_4$ phase. Additionally, we obtained the

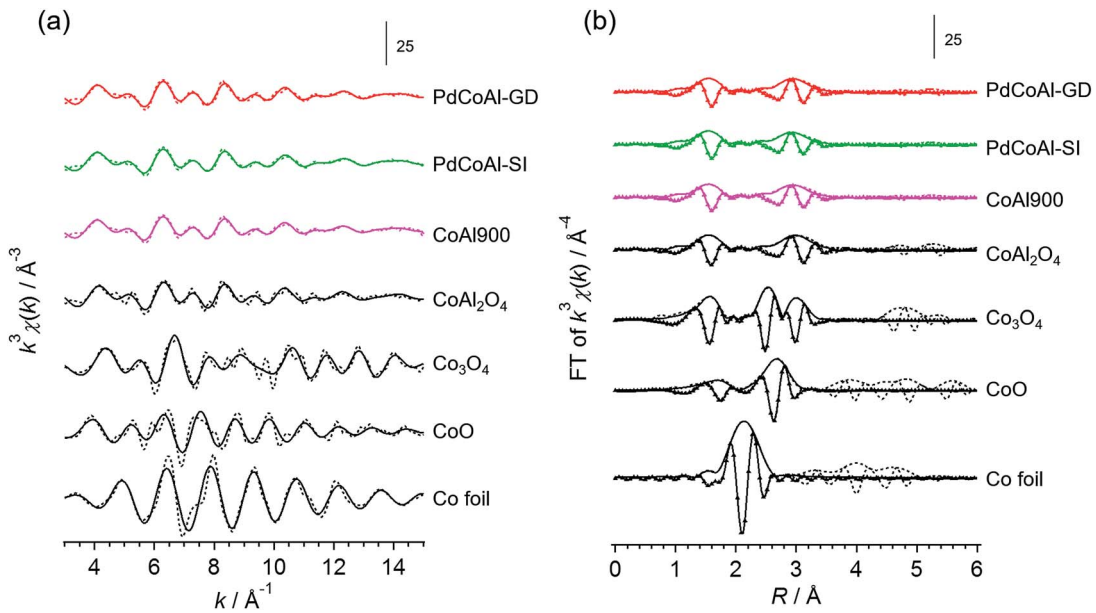

Fig. 4 (a) k^3-weighted Co K-edge EXAFS spectra and (b) Fourier transform of PdCoAl-GD (red), PdCoAl-SI (green), CoAl900 (pink) and references (black). Dotted lines: raw data; solid line: fitting data; marked: imaginary part of the Fourier transform.

Open Access Article. Published on 11 July 2017. Downloaded on 1/9/2026 1:23:19 AM.
This article is licensed under a Creative Commons Attribution-NonCommercial 3.0 Unported Licence.

Table 3 Curve-fitting results of the k^3-weighted Co K-edge EXAFS data for PdCoAl-GD

Sample	Shell	CN	R/Å	$\sigma^2/10^4$ nm^2
PdCoAl-GD[a]	Co–O	3.8 ± 0.9	1.96 ± 0.01	0.37 ± 0.19
	Co–Al	7.7 ± 2.0	3.37 ± 0.08	0.89 ± 2.80
	Co–O	7.7 ± 2.0	3.40 ± 0.08	0.39 ± 2.43
	Co–Co	2.6 ± 0.7	3.51 ± 0.08	0.63 ± 1.31

[a] $\Delta E = 1.99$ eV, $R_{factor} = 4\%$.

Co 2p X-ray photoelectron spectroscopy (XPS) spectra of all the samples (Fig. S3†). Therefore, $CoAl_2O_4$ species were considered to be present near the surface of γ-Al_2O_3.

Fig. 5 shows HAADF-STEM and EDX elemental mapping images of PdCoAl-GD, PdCoAl-SI and PdAl-I. The white contrast in the HAADF-STEM images was produced by the Pd nanoparticles, while the green, yellow and red regions in the EDX elemental mapping were ascribed to Al, Co and Pd, respectively. In the case of PdCoAl-GD and PdCoAl-SI, the Co species were mainly overlapped with those of Al. According to the Co K-edge XAFS spectra, PdCoAl-GD and PdCoAl-SI possessed a $CoAl_2O_4$ phase dispersed over γ-Al_2O_3. In the case of PdCoAl-GD, Pd species with a size of 2–7 nm were detected overlapping with Al and Co species. Since GD proceeds upon contact between a Pd precursor and reduced Co species, Pd nanoparticles were deposited onto $CoAl_2O_4$ species. The Pd size distributions were obtained by analyzing the HAADF-STEM images (Fig. 5). The average Pd particle size calculated by STEM was in rough agreement with that estimated by CO chemisorption (Table 1) However, the enhanced activity cannot be explained only by characterizing the catalyst before methane combustion. A detailed analysis of the state of Pd during reaction is necessary.

Operando Pd K-edge XAFS measurements

We performed operando Pd K-edge XAFS measurements to clarify the Pd oxidation state during methane combustion. The samples were analyzed at the same conditions used for the catalytic tests including a H_2 pretreatment (see Fig. 1). Fig. 6 shows a series of normalized Pd K-edge XANES spectra of PdCoAl-GD. First, after the oxidation pretreatment, Pd was in form of PdO (Fig. 6(b)). Pd was subsequently reduced to Pd^0 after the H_2 pretreatment (Fig. 6(c)). Pd was slightly oxidized when contacted with flowing reaction gases at 200 °C (Fig. 6(d)). The fraction of PdO gradually increased with temperature until complete oxidation of Pd. Similar operando XAFS measurements were conducted for PdCoAl-SI and PdAl-I (Fig. S4 and S5†). All Pd K-edge XANES spectra were described with a linear combination fitting (LCF) of two XANES spectra *i.e.*, the one obtained after oxidation at 500 °C (Fig. 6(b)), and that obtained after reduction at 500 °C (Fig. 6(c)). The amount of PdO (PdO ratio) in the catalysts was estimated using LCF. During the XAFS measurements, the outlet gases were analyzed by MS, and the CH_4 conversion was calculated with the reaction temperature. Fig. 7(a)–(c) show the PdO ratio and CH_4 conversion values under reaction for PdCoAl-GD, PdCoAl-SI and PdAl-I. In the case of PdCoAl-GD, the CH_4 conversion increased with the PdO ratio (900 s, reaction temperature: 275 °C). A similar trend was found for PdCoAl-SI and PdAl-I, although CH_4 conversion and PdO

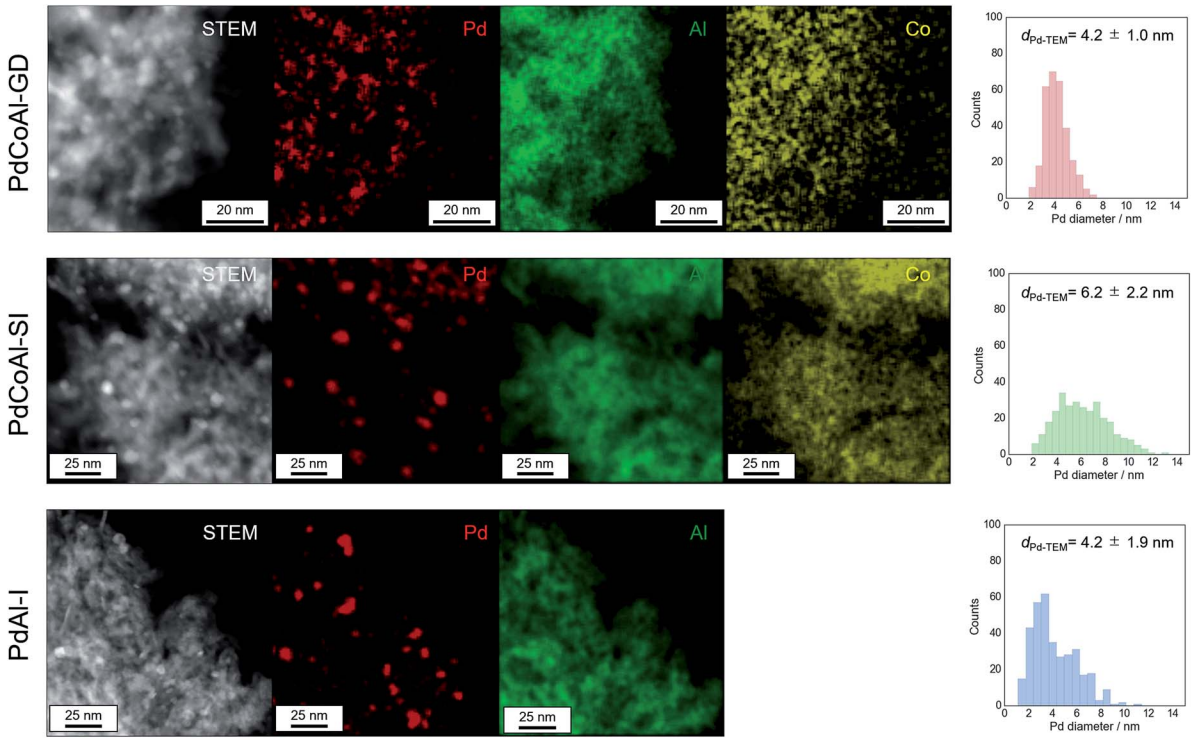

Fig. 5 HAADF-STEM images, EDX element mapping, and Pd particle size histograms for PdCoAl-GD, PdCoAl-SI, and PdAl-I.

Open Access Article. Published on 11 July 2017. Downloaded on 1/9/2026 1:23:19 AM.
This article is licensed under a Creative Commons Attribution-NonCommercial 3.0 Unported Licence.

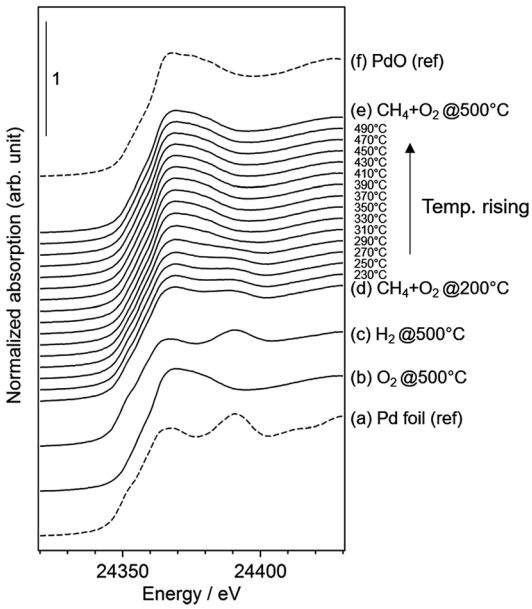

Fig. 6 Normalized Pd K-edge XANES spectra of: (a) Pd foil as a reference; (b–e) results for PdCoAl-GD under operando XAFS measurements; (f) PdO as a reference.

formation were observed at higher temperatures. Moreover, we performed operando XAFS studies for several Pd/Al_2O_3 catalysts having different catalytic activities (Table S2 and Fig. S6†). As shown in Fig. 7(d), the relationship between T_{10} and the PdO ratio at 310 °C was roughly linear for all the catalysts. The catalysts with higher PdO contents showed lower T_{10} values. Considering the operando XAFS measurements above described, PdO was the main active species. Thus, the low light-off temperature of PdCoAl-GD can be ascribed to the oxidation of Pd^0 to PdO at low temperatures.

Methane combustion over PdO state catalysts

As indicated in the previous section, the main active species for this reaction is PdO. This result led us to make the following question: What would happen if Pd was initially in form of PdO? Would the catalysts show similar catalytic activities?

Fig. 8 shows the methane combustion results of the catalysts previously treated with O_2 with the aim to oxidized Pd to PdO. Although Pd was initially as PdO, PdCoAl-GD showed the highest activity among all the catalysts tested. When Pd was initially as Pd^0, PdCoAl-SI and PdAl-I showed different trends above 300 °C (Fig. 1) in virtue of their Pd particle size (6.3 *vs.* 3.8 nm, respectively). Pd was gradually oxidized during the catalytic tests such that PdO was main active species in this reaction. Since the Pd surface area of PdCoAl-SI was lower than that of PdAl-I, the former material was considered to have lower Pd oxidation rates. As indicated in Fig. 8, the activity of the catalysts having PdO as the initial phase followed the trend PdCoAl-GD > PdCoAl-SI > PdAl-I in all the temperature ranges.

The rate-limiting step for methane combustion on PdO is the activation of the C–H bond in CH_4 that takes place at the beginning of the reaction.[44,45] In this step, the PdO surface is partially reduced by the CH_4 molecule. Thus, to investigate the reducibility of PdO, CH_4-TPR measurement was conducted

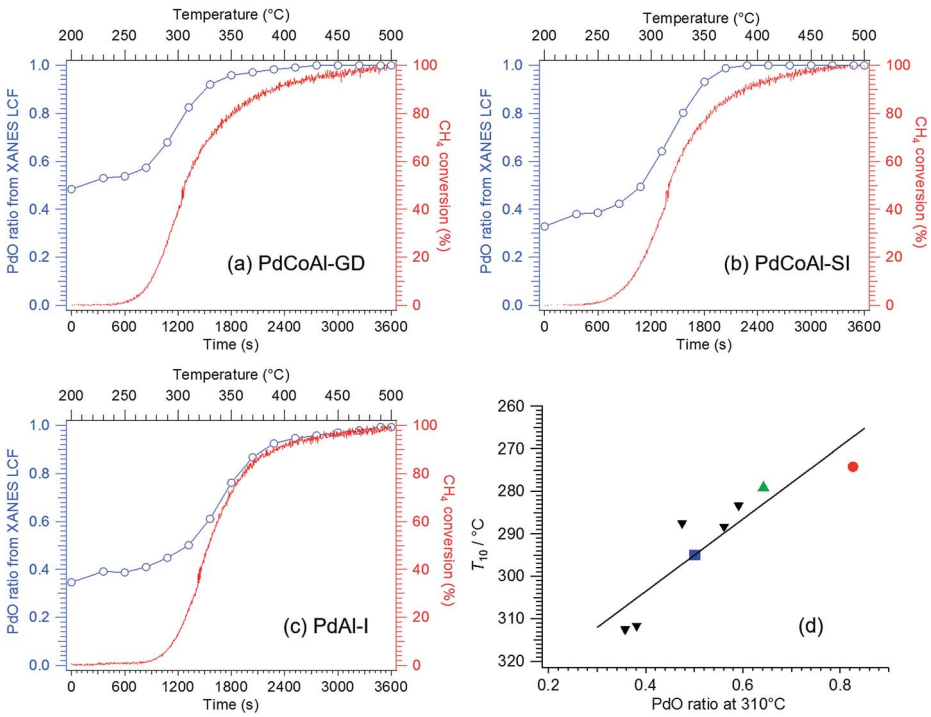

Fig. 7 PdO ratio and CH_4 conversion as a function of time for: (a) PdCoAl-GD, (b) PdCoAl-SI and (c) PdAl-I during operando XAFS measurements. (d) Correlation between T_{10} and the PdO ratio at 310 °C over Pd-based catalysts. Red circle: PdCoAl-GD; green triangle: PdCoAl-SI; blue square: PdAl-I; black down-pointing triangle; series of Pd/Al_2O_3 (see Fig. S6†).

Open Access Article. Published on 11 July 2017. Downloaded on 1/9/2026 1:23:19 AM.
This article is licensed under a Creative Commons Attribution-NonCommercial 3.0 Unported Licence.

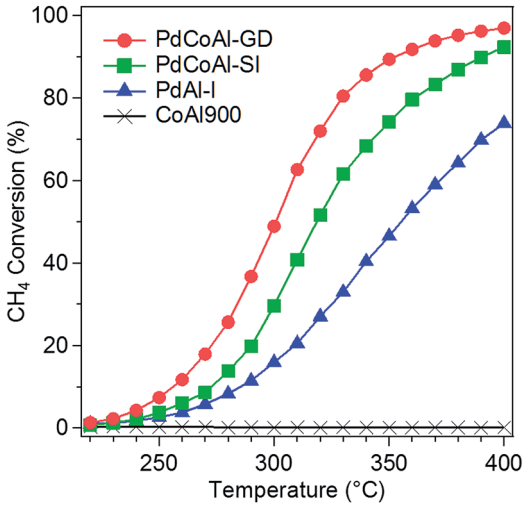

Fig. 8 Methane combustion light-off curves of: PdCoAl-GD, PdCoAl-SI, PdAl-I and CoAl900. Pretreatment: flowing O_2 at 500 °C.

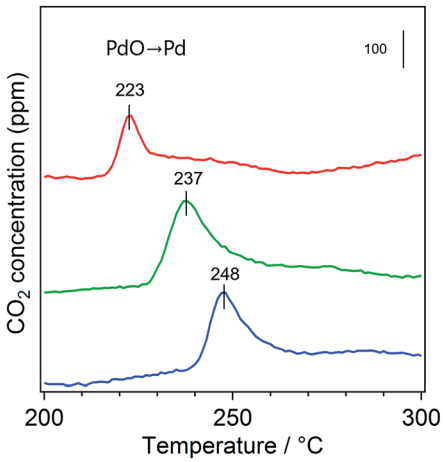

Fig. 9 CH_4-TPR results for: PdCoAl-GD (red), PdCoAl-SI (green) and PdAl-I (blue).

shown as Fig. 9. The PdO nanoparticles of PdCoAl-GD were reduced by CH_4 at a lower temperature as compared to PdCoAl-SI and PdAl-I (by 14 and 25 °C, respectively). This trend was similar to that of the catalytic activities (Fig. 8). The CH_4-TPR results indicated the activity of PdO toward the activation of the C–H bond was improved in PdCoAl-GD as compared to PdCoAl-SI and PdAl-I. This enhancement can be explained as follows. According to the Pd 3d XPS results, the Pd $3d_{5/2}$ XPS peak of PdCoAl-GD was different for the catalysts prepared herein (Fig. 10). In the case of PdAl-I, the Pd $3d_{5/2}$ XPS peak was fitted with a peak almost derived from Pd^{2+}. In the case of PdCoAl-SI and PdCoAl-GD, a good fit was not obtained with only one peak derived from Pd^{2+}, and the presence of a peak derived from Pd^{n+} ($0 < n < 2$) was confirmed. In the case of PdCoAl-GD, which showed the highest catalytic activity, the binding energy of Pd^{n+} shifted to the lower energy side, and the ratio of Pd^{n+} was the largest among the catalysts tested. These results suggest that

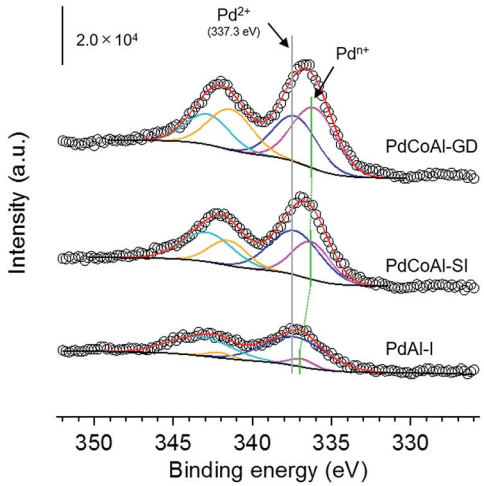

Fig. 10 Pd 3d XPS spectra of PdCoAl-GD, PdCoAl-SI, and PdAl-I. Circle, raw data; blue, Pd^{2+} $3d_{5/2}$; cyan, Pd^{2+} $3d_{3/2}$; pink, Pd^{n+} $3d_{5/2}$; yellow, Pd^{n+} $3d_{3/2}$; red, sum of fitting; black, background.

the electronic state of PdO changed as a result of the interaction with $CoAl_2O_4$, becoming electron enriched. Thus, the contact of PdO and $CoAl_2O_4$ can alter the electron states of PdO, resulting in enhanced C–H activation.

Conclusion

$Pd/CoAl_2O_4/Al_2O_3$ catalysts prepared by a GD method (PdCoAl-GD) showed high activity toward the methane combustion reaction. PdCoAl-GD was comprised of a $CoAl_2O_4$ phase on γ-Al_2O_3 and dispersed Pd nanoparticles of 2–7 nm in size on a $CoAl_2O_4$ phase. Operando XAFS measurements revealed that the light-off temperature decreased for the PdO phase (*i.e.*, the main active species) generated at lower temperatures. Furthermore, PdCoAl-GD showed the highest methane combustion activity among the catalysts tested herein even when PdO was initially present on the catalysts. As revealed by CH_4-TPR, PdO in PdCoAl-GD was reduced at low temperatures by CH_4. PdO species of the catalyst prepared by GD method were effective in activating the C–H bond of CH_4. GD is a simple preparation method comparable to conventional impregnation approaches. Thus, further research on the industrial applications of GD catalysts and mechanism elucidation should be carried out.

Acknowledgements

This work was supported by Grant-in-Aids from the Ministry of Education, Culture, Sports, Science and Technology (MEXT), Japan, "Elements Strategy Initiative to Form Core Research Center" program, and Grants-in-Aid for Scientific Research KAKENHI (B) (15H04186). The XAFS measurements at the SPring-8 were carried out through the approval (proposal no. 2015B1482, 2016A1662) of Japan Synchrotron Radiation Research Institute (JASRI).

Open Access Article. Published on 11 July 2017. Downloaded on 1/9/2026 1:23:19 AM.
This article is licensed under a Creative Commons Attribution-NonCommercial 3.0 Unported Licence.

References

1 R. J. Farrauto, *Science*, 2012, **337**, 659–660.
2 P. Gélin and M. Primet, *Appl. Catal., B*, 2002, **39**, 1–37.
3 T. V. Choudhary, S. Banerjee and V. R. Choudhary, *Appl. Catal., A*, 2002, **234**, 1–23.
4 X. Zou, Z. Rui and H. Ji, *ACS Catal.*, 2017, **7**, 1615–1625.
5 Y. Lou, J. Ma, W. Hu, Q. Dai, L. Wang, W. Zhan, Y. Guo, X.-M. Cao, Y. Guo, P. Hu and G. Lu, *ACS Catal.*, 2016, **6**, 8127–8139.
6 J. Shen, R. E. Hayes, X. Wu and N. Semagina, *ACS Catal.*, 2015, **5**, 2916–2920.
7 S. Colussi, A. Gayen, M. F. Camellone, M. Boaro, J. Llorca, S. Fabris and A. Trovarelli, *Angew. Chem., Int. Ed.*, 2009, **48**, 8481–8484.
8 K. Sekizawa, H. Widjaja, S. Maeda, Y. Ozawa and K. Eguchi, *Appl. Catal., A*, 2000, **200**, 211–217.
9 R. J. Farrauto, M. C. Hobson, T. Kennelly and E. M. Waterman, *Appl. Catal., A*, 1992, **81**, 227–237.
10 M. Lyubovsky and L. Pfefferle, *Appl. Catal., A*, 1998, **173**, 107–119.
11 Z. Chen, S. Wang, Y. Ding, L. Zhang, L. Lv, M. Wang and S. Wang, *Appl. Catal., A*, 2017, **532**, 95–104.
12 C. L. Pieck, C. R. Vera, E. M. Peirotti and J. C. Yori, *Appl. Catal., A*, 2002, **226**, 281–291.
13 Y. Liu, S. S. Wang, T. Sun, D. Gao, C. Zhang and S. S. Wang, *Appl. Catal., B*, 2012, **119–120**, 321–328.
14 L. M. T. Simplício, S. T. Brandão, E. A. Sales, L. Lietti and F. Bozon-Verduraz, *Appl. Catal., B*, 2006, **63**, 9–14.
15 M. Monai, T. Montini, M. Melchionna, T. Duchoň, P. Kúš, C. Chen, N. Tsud, L. Nasi, K. C. Prince, K. Veltruská, V. Matolín, M. M. Khader, R. J. Gorte and P. Fornasiero, *Appl. Catal., B*, 2017, **202**, 72–83.
16 H. Yoshida, T. Nakajima, Y. Yazawa and T. Hattori, *Appl. Catal., B*, 2007, **71**, 70–79.
17 R. Burch and P. K. Loader, *Appl. Catal., B*, 1994, **5**, 149–164.
18 B. Yue, R. Zhou, Y. Wang and X. Zheng, *Appl. Surf. Sci.*, 2006, **252**, 5820–5828.
19 H. Liao, M. Liu and P. Zuo, *Catal. Commun.*, 2016, **76**, 62–66.
20 J. H. Park, J. H. Ahn, H. I. Sim, G. Seo, H. S. Han and C. H. Shin, *Catal. Commun.*, 2014, **56**, 157–163.
21 Y. Mahara, J. Ohyama, T. Tojo, K. Murata, H. Ishikawa and A. Satsuma, *Catal. Sci. Technol.*, 2016, **6**, 1–10.
22 Z. Wang, J. Deng, Y. Liu, H. Yang, S. Xie, Z. Wu and H. Dai, *Catal. Today*, 2017, **281**, 467–476.
23 A. Satsuma, T. Tojo, K. Okuda, Y. Yamamoto, S. Arai and J. Oyama, *Catal. Today*, 2015, **242**, 308–314.
24 G. Ercolino, G. Grzybek, P. Stelmachowski, S. Specchia, A. Kotarba and V. Specchia, *Catal. Today*, 2015, **257**, 66–71.
25 H. Widjaja, K. Sekizawa, K. Eguchi and H. Arai, *Catal. Today*, 1997, **35**, 197–202.
26 G. Guo, K. Lian, F. Gu, D. Han and Z. Wang, *Chem. Commun.*, 2014, **50**, 13575–13577.
27 G. Di Carlo, G. Melaet, N. Kruse, L. F. Liotta, G. Pantaleo and A. M. Venezia, *Chem. Commun.*, 2010, **46**, 6317–6319.
28 P. Stefanov, S. Todorova, A. Naydenov, B. Tzaneva, H. Kolev, G. Atanasova, D. Stoyanova, Y. Karakirova and K. Aleksieva, *Chem. Eng. J.*, 2015, **266**, 329–338.
29 H. Nassiri, K.-E. Lee, Y. Hu, R. E. Hayes, R. W. J. Scott and N. Semagina, *ChemPhysChem*, 2017, **18**, 238–244.
30 Y. Liu, S. Wang, D. Gao, T. Sun, C. Zhang and S. Wang, *Fuel Process. Technol.*, 2013, **111**, 55–61.
31 Z. Wu, J. Deng, Y. Liu, S. Xie, Y. Jiang, X. Zhao, J. Yang, H. Arandiyan, G. Guo and H. Dai, *J. Catal.*, 2015, **332**, 13–24.
32 X. Zou, Z. Rui, S. Song and H. Ji, *J. Catal.*, 2016, **338**, 192–201.
33 X. Pan, Y. Zhang, Z. Miao and X. Yang, *J. Energy Chem.*, 2013, **22**, 610–616.
34 N. M. Kinnunen, J. T. Hirvi, M. Suvanto and T. A. Pakkanen, *J. Mol. Catal. A: Chem.*, 2012, **356**, 20–28.
35 G. Zhu, J. Han, D. Y. Zemlyanov and F. H. Ribeiro, *J. Am. Chem. Soc.*, 2004, **126**, 9896–9897.
36 M. Cargnello, J. J. D. Jaen, J. C. H. Garrido, K. Bakhmutsky, T. Montini, J. J. C. Gamez, R. J. Gorte and P. Fornasiero, *Science*, 2012, **337**, 713–717.
37 A. Y. Stakheev, A. M. Batkin, N. S. Teleguina, G. O. Bragina, V. I. Zaikovsky, I. P. Prosvirin, A. K. Khudorozhkov and V. I. Bukhtiyarov, *Top. Catal.*, 2013, **56**, 306–310.
38 M. Monai, T. Montini, M. Melchionna, T. Duchoň, P. Kúš, N. Tsud, K. Prince, V. Matolin, R. J. Gorte and P. Fornasiero, *Appl. Catal., B*, 2015, **197**, 271–279.
39 T. P. Senftle, A. C. T. van Duin and M. J. Janik, *ACS Catal.*, 2017, **7**, 327–332.
40 Y. Mahara, H. Ishikawa, J. Ohyama, K. Sawabe and A. Satsuma, *Catal. Today*, 2016, **265**, 2–6.
41 Y. Mahara, H. Ishikawa, J. Ohyama, K. Sawabe, Y. Yamamoto, S. Arai and A. Satsuma, *Chem. Lett.*, 2014, **43**, 910–912.
42 J. Ohyama, H. Ishikawa, Y. Mahara, T. Nishiyama and A. Satsuma, *Bull. Chem. Soc. Jpn.*, 2016, **89**, 914–921.
43 H. Wang, C. Chen, Y. Zhang, L. Peng, S. Ma, T. Yang, H. Guo, Z. Zhang, D. S. Su and J. Zhang, *Nat. Commun.*, 2015, **6**, 7181.
44 Y. C. Chin, M. García-Diéguez and E. Iglesia, *J. Phys. Chem. C*, 2016, **120**, 1446–1460.
45 Y. H. Chin, C. Buda, M. Neurock and E. Iglesia, *J. Am. Chem. Soc.*, 2013, **135**, 15425–15442.